Progress In Electromagnetics Research C, Vol. 79, 115–126, 2017

High Gain Slotted Waveguide Antenna Based on Beam Focusing Using Electrically Split Ring Resonator Metasurface Employing Negative Refractive Index Medium

Adel A. A. Abdelrehim and Hooshang Ghafouri-Shiraz*

Abstract—In this paper, a new high performance slotted waveguide antenna incorporated with negative refractive index metamaterial structure is proposed, designed and experimentally demonstrated. The metamaterial structure is constructed from a multilayer two-directional structure of electrically split ring resonator which exhibits negative refractive index in direction of the radiated wave propagation when it is placed in front of the slotted waveguide antenna. As a result, the radiation beams of the slotted waveguide antenna are focused in both E and H planes, and hence the directivity and the gain are improved, while the beam area is reduced. The proposed antenna and the metamaterial structure operating at 10 GHz are designed, optimized and numerically simulated by using CST software. The effective parameters of the eSRR structure are extracted by Nicolson Ross Weir (NRW) algorithm from the s-parameters. For experimental verification, a proposed antenna operating at 10 GHz is fabricated using both wet etching microwave integrated circuit technique (for the metamaterial structure) and milling technique (for the slotted waveguide antenna). The measurements are carried out in an anechoic chamber. The measured results show that the E plane gain of the proposed slotted waveguide antenna is improved from 6.5 dB to 11 dB as compared to the conventional slotted waveguide antenna. Also, the E plane beamwidth is reduced from 94.1 degrees to about 50 degrees. The antenna return loss and bandwidth are slightly changed. Furthermore, the proposed antenna offered easier fabrication processes with a high gain than the horn antenna, particularly if the proposed antenna is scaled down in dimensionality to work in the THz regime.

1. INTRODUCTION

During the last two decades, metamaterials (MTMs) have received great attention due to their fascinating electromagnetic (EM) properties. MTMs are artificial atoms which exhibit exotic EM properties that cannot be achieved by the natural materials. MTMs can provide negative, zero or positive electric permittivity and magnetic permeability by inserting inclusion with specific geometrical shape and dimensionality in a host medium, and both of the inclusions and the host medium are constructed from metals and dielectrics [1]. There are two main categories for the MTMs which are resonance and non-resonance [2, 3], and each group has its own advantages and disadvantages and can be used to develop nowadays practical applications. Recently, MTMs with simultaneously negative permittivity, permeability and negative index of refraction are used to design perfect lenses [4, 5] for high resolution imaging system and to design many antennas [6, 7]. Also, MTMs are proposed to design gradient index of refraction lenses [8], absorbing, cloaking [9, 10], polarization transformer [11]. By using MTMs with negative or gradient index of refraction, compact size, high directive antennas

Received 7 February 2017, Accepted 30 September 2017, Scheduled 5 November 2017

* Corresponding author: Hooshang Ghafouri-Shiraz (ghafourh@bham.ac.uk).
The authors are with the School of Electronic, Electrical and System Engineering, University of Birmingham, Birmingham, B15 2TT, United Kingdom.

can be designed [12, 13]. It is well know that high directive antennas play an important role in many practical applications. Many conventional efforts have been made to improve the antenna directivity such as parasitic patches, array of patch antennas, and parabolic reflectors [14–16]. Unfortunately, the aforementioned approaches suffer from large sizes, design methodology, complex feeding network and fabrication processes, particularly in the high frequencies. As Pendry investigated the first negative refractive index perfect lens (i.e., double negative MTMs with simultaneously negative permittivity, permeability and negative index of refraction) in 2000 [17], it is possible to design a compact size and high directive antennas [18, 19]. Furthermore, metamaterial structures composed of 3-D metal grid superstrates have been used to improve the directivity of the antennas [20, 21]. It should be noted that the aperture size of the metamaterial superstrate is much bigger than the size of the patch which makes the antenna very bulky. Also, a zero index medium metamaterial superstrate is used to develop a high gain and wideband antenna [22]. It is clear from the structure of the antenna that the metamaterial superstrate uses via to resemble shunt inductance, which makes it difficult in fabrication. The photonic crystal-based resonant antenna presented in [23] is a high directive antenna, but it is very bulky and has a narrow bandwidth. Engheta and his research team proved numerically and theoretically that a PEC screen with small hole covered by two subwavelength metamaterial structures can be used to improve the directivity of the antenna [24]. Planar metamaterial with NRI has been developed using split ring resonator (SRR) in [25].

This work focuses on two interesting contributions. Firstly, a 2D single sided metasurface structure based on an electrically split ring resonator (eSRR) [26] is designed by choosing proper dimensionality and orientation such that it exhibits NRI property in the direction of the wave propagation, and hence it can be used to improve the directivity of the EM emission. This 2D metasurface structure has the advantage of easier fabrication and assembly processes over the volumetric MTMs (mentioned in [20–22]), so it can be scaled down to be fabricated for THz antennas for high resolution imaging and biomedical application (e.g., heart beat measurements). Secondly, a slotted waveguide antenna [27] is used as EM radiator instead of horn antenna or patch antenna because it is difficult to design a horn antenna with flared surfaces in the THz regime. Furthermore, there are no SMA connectors for the patch antenna operating in the THz regime. Fortunately, for waveguide, there are waveguide connectors up to 900 GHz [28, 29]. Thus the only solution to design a THz antenna is to use waveguide fed or photo conductive antennas. Here, we use the waveguide to feed the slotted antenna. Due to the low gain of the single element slotted antenna (the typical gain is 6.5 dB), NRI medium is used as a superstrate to improve the transverse electromagnetic (TEM) wave radiated from the slotted waveguide antenna, and hence the E and H plane gains and directivities are improved. For experimental verification, the slotted waveguide antenna incorporated with eSRR NRI medium operating at 10 GHz is designed, numerically optimized in CST software, fabricated and measured.

This paper is organized as follows. Section 2 provides the design and simulation of a 10 GHz conventional slotted antenna. Section 3 discusses the design and effective parameter extraction of NRI medium based on eSRR. Section 4 presents the design and numerical simulation of the 10 GHz slotted waveguide antenna incorporated with NRI medium. In section 5, experimental verifications for the proposed antenna are carried out. Finally, the conclusion and future recommendations are given in section 6.

2. DESIGN AND SIMULATION OF 10 GHZ SLOTTED WAVEGUIDE ANTENNA

According to Babinet's principle, in order to form aperture radiator, a slot of length L_s and width W_s can be cut in the side wall, top wall or even in the back wall of a waveguide [30]. Here, a conventional 10 GHz slotted waveguide antenna is designed and simulated using Finite Element based Electromagnetic CST simulator. Fig. 1 illustrates the structure of the antenna; the antenna is constructed from WR-90 waveguide of standard dimensions a and b of 22.86 mm and 10.16 mm, respectively. The slot is cut in the back wall of the waveguide. The slot dimensions are designed properly such that the antenna operates at 10 GHz and has a good impedance matching with the free space; the slot length is about free space half wavelength. Three different slotted antennas of back wall slots of dimensions (L_s, W_s) of (14.5, 2), (14.7, 4), and (15.2, 6) are designed, and all dimensions are in mm. The waveguide has length L_{wg} of 30 mm which equals one free space wavelength at the operating frequency of 10 GHz and

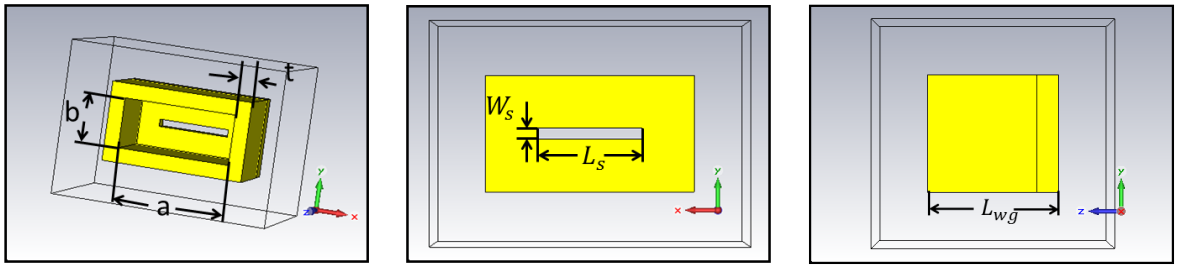

(a) (b) (c)

Figure 1. Conventional waveguide slotted antenna, (a) 3-D view, (b) back view and (c) side view.

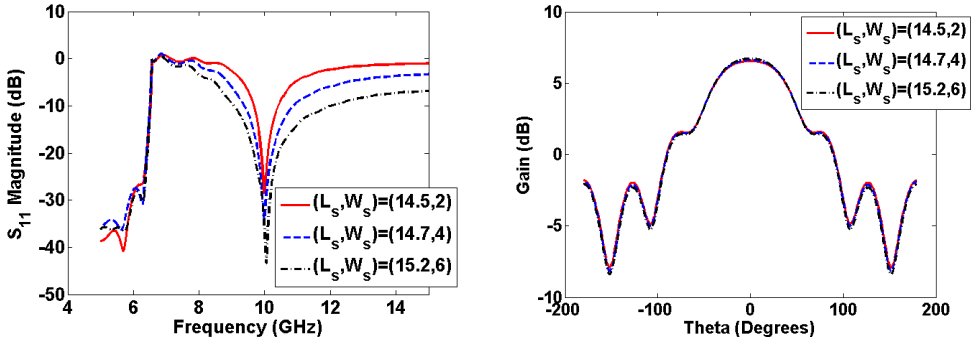

(a) (b)

Figure 2. Conventional 10 GHz slotted waveguide antenna performance at different slot dimensions of length L_s and width W_s, all dimensions are in mm, (a) return loss S_{11} in dB and (b) E-palne Gain in dB.

thickness 3 mm to match the requirements of the fabrication, mechanical, and assembly processes. The antenna is simulated in CST software; the return loss S_{11} and gain are extracted as shown in Fig. 2. It is clear from Fig. 2 that when the slot width W_s increases, and the slot length L_s is changed slightly around the free space half wavelength of 15 mm at 10 GHz to keep the operating frequency at 10 GHz, the gain slightly decreases, while the bandwidth increases. Furthermore, the results illustrate that for slotted waveguide antennas of slot widths W_s of 2, 4, and 6 mm and slot lengths L_s of 14.5, 14.7 and 15.2 mm, the bandwidths are 0.72, 1.5 and 2.88 GHz, respectively, and the gain is about 6.5 dB mostly for all the three slot dimensions.

3. DESIGN AND SIMULATION OF 10 GHZ NEGATIVE REFRACTIVE INDEX LAYER BASED ON ESRR

Here, a unit cell of an Electrically Split Ring Resonator (eSRR) metasurface structure is designed and simulated in CST. The eSRR unit cell is optimized and repeated in two dimensions which may provide electric and magnetic plasmonic resonances around 10 GHz and hence exhibits simultaneous negative permittivity, permeability and index of refraction. The eSRR metasurface is a copper layer with thickness t of 35 µm mounted on the top side of an RT/Duriod 5880 dielectric substrate with relative dielectric permittivity εr of 2.2 and height $h = 1.57$ mm. The eSRR is shown in Fig. 3 with physical dimensions; a, L, d, g and w of 5.5, 5.3, 2.8, 0.3 and 0.62, respectively. All dimensions are in mm. Then, the eSRR unit cell is simulated in CST software using Floquet's boundaries conditions of unit cells in the x and y directions. The structure is excited by TEM plane wave propagating in the z-direction, with incident electric field polarized in x direction and incident magnetic field polarized in y direction as shown in Fig. 3(b). The scattering parameters of the metasurface structure are calculated, extracted and plotted as shown in Fig. 4(a). Fig. 4(a) shows that the eSRR metasurface infinite periodicity unit

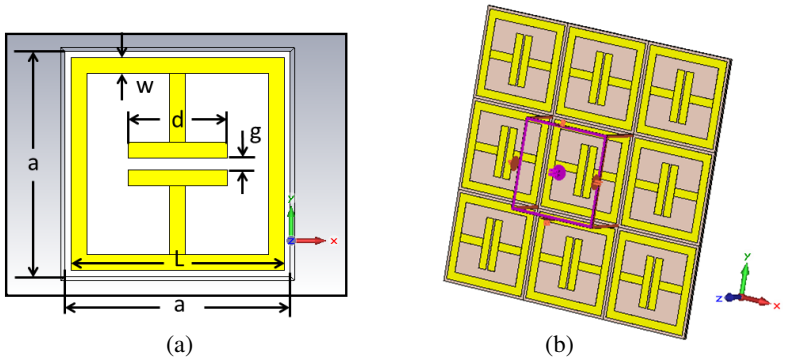

Figure 3. The eSRR metasurface structure, (a) 3-D view with unit cell boundary conditions in x-y plane and the excitation in z direction, and (b) front view of MTM unit cell with unit cells infinite periodicities in x and y directions.

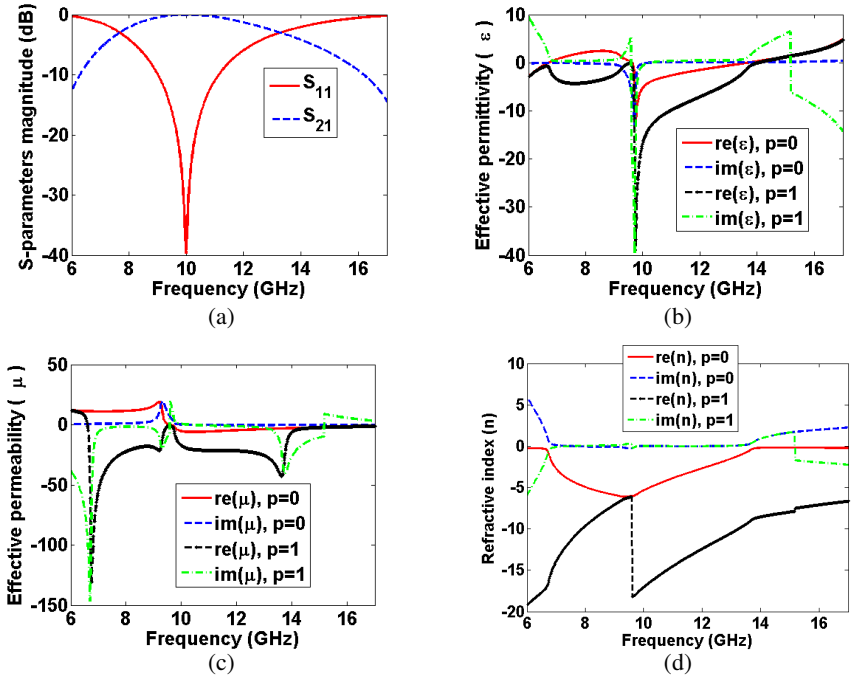

Figure 4. The eSRRs infinite 2-D periodicity metasurface structure with negative effective parameters around 10 GHz, extracted at two different unambiguity branch parameter p of 0 and 1 [32] (a) S-parameters magnitude. (b) Effective permittivity (ε), Effective permeability (μ) and refractive index (n). The real part of effective parameters at $p = 1$ are plotted with dotted lines.

cell has a band-pass response with center frequency around 10 GHz.

Then the effective parameters of the metasurface unit cell with infinite periodicity have been extracted from the S-parameters using Nicolson-Ross-Weir (NRW) approach [31–35], and the results are plotted as shown in Figs. 4(b), (c) and (d), respectively for two different branch ambiguity factors p of 0 and 1 values. According to the theory developed in [32], the correct branch ambiguity factor for this MTM structure is $p = 0$ since it is a thin MTM slab.

Figures 4(b), (c) and (d) show that the real parts of the effective permittivity ε', effective permeability μ' and effective refractive index n', respectively, are negative around the resonance frequency of 10 GHz at $p = 0$. In [32], the authors proved that the MTM effective parameters extraction based on the S-parameters method has no ambiguity related to the sign of the wavenumber k_s and the

intrinsic impedance η_s of the metamaterials layer, while it has ambiguities related to the branch of the complex logarithm. Based on this method, the effective permittivity ε_s and effective permeability μ_s are given as follows:

$$\varepsilon_s = \frac{k_s}{\omega \eta_s} \tag{1}$$

$$\varepsilon = \varepsilon' + j\,\varepsilon'' = \frac{\varepsilon_s}{\varepsilon_0} \tag{2}$$

where ε' and ε'' are the real and imaginary parts of the relative (effective) permittivity of the MTM slab, respectively; ε is the MTM slab relative permeability; ε_0 is the free space permittivity.

$$\mu_s = \frac{k_s \eta_s}{\omega} \tag{3}$$

$$\mu = \mu' + j\,\mu'' = \frac{\mu_s}{\mu_0} \tag{4}$$

where μ' and μ'' are the real and imaginary parts of the relative (effective) permeability of the MTM slab, respectively; μ is the MTM slab relative permeability; μ_0 is the free space permeability.

The intrinsic impedance in the MTM layer η_s can be calculated from the free space intrinsic impedance η_0 which is $120\pi\,\Omega$ and the MTM S-parameters as follows:

$$\eta_s = \pm\,\eta_0 \sqrt{\frac{(S_{11}+1)^2 - S_{21}^2}{(S_{11}-1)^2 - S_{21}^2}} \tag{5}$$

The wavenumber k_s inside the MTM layer of thickness d can be expressed as follow:

$$k_s = \frac{j}{d}\log(Z) = \frac{1}{d}\left(-\left(Arg\,(Z) + 2\pi p\right) + j\,\log(Z)\right) \tag{6}$$

$$Z = \frac{S_{21}(\eta_s + \eta_0)}{(\eta_s + \eta_0) - S_{11}(\eta_s - \eta_0)} \tag{7}$$

The term $2\pi p$ (where p is an integer number) defines the branches of $\log Z$, and there is a specific value of p giving the branch ambiguity in the real part of k_s which is k_s'. It has been noticed that there is no branch ambiguity in the imaginary part of k_s which is k_s''. The branch ambiguity factor p is determined based on the geometry of the MTM slab, whether it is thin, thick or multi-layered. In our case, the MTM slab is thin, since the relation between the wavelength λ_s of 30 mm at the predefined interesting frequency which is 10 GHz and the thickness d of the MTM slab which is 1.6 mm is $\lambda_s > 2d$. As a result, $|k_s'|\,d < \pi$, and therefore, Arg (Z) is limited to the interval $[-\pi, \pi]$, so p is set to 0 in Equation (6). Thus, the material parameters can be extracted unambiguously for electrically thin slab which is the case of this paper. This means that there is limitation for applying the NRW algorithm in extracting the effective parameters of eSSR MTM resonating at high frequency, since the NRW algorithm can be used to extract the effective parameters of the eSRR MTM only if the fundamental branch of the complex logarithm is selected throughout the entire frequency range. Moreover, if the frequency is changed, shift of branch from the fundamental to the next higher order branch is required to enable the NRW algorithm to extract the effective parameters, in order to ensure the continuous material parameters [32].

The impact on infinite periodicity truncation of the metasurface structure on the effective parameters is studied by designing an eSRR metasurface structure of size $3 \times 6 \times 2$ with negative effective parameters around 10 GHz. After truncation, the dimensions of the eSRR unit cell is optimized such that the structure still has negative effective parameters around 10 GHz. The dimensions of the truncated periodicity eSRR metasurface are; $a = 3.75$ mm, $L = 3.525$ mm, $d = 1.75$ mm, $g = 0.3$ mm and $w = 0.496$ mm. The truncated periodicity eSRR metasurface structure is designed and simulated in CST; the S-parameters are extracted and plotted as shown in Fig. 5(a). The S-parameters show that the structure still has a band pass response at 10 GHz. Then the effective parameters are extracted and plotted as shown in Figs. 5(b) to (d) from the S-parameters using the NRW algorithm at different non-ambiguity branches of $p = 0$ and $= 1$. It is clear from Fig. 5 that at $p = 0$ which is the correct branch according to the theory developed in [32], the structure still has simultaneous negative real effective parameters around 10 GHz. It means that the eSRR structure of size $3 \times 6 \times 2$ exhibits NRI, so it can focus the radiated EM waves from the slotted waveguide antenna.

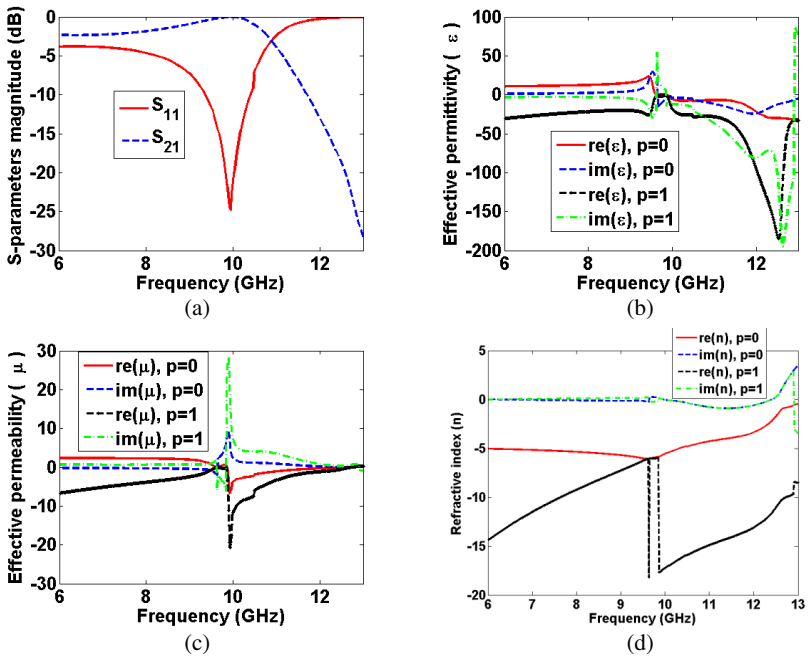

Figure 5. The eSRR metasurface structure with truncated periodicity with finite sizes of $3 \times 6 \times 2$ with negative effective parameters around 10 GHz, extracted at two different unambiguity branch parameter p of 0 and 1 [32] (a) Magnitude of the scattering parameters. (b) Effective permittivity (ε), Effective permeability (μ) and refractive index (n).

4. DESIGN AND SIMULATION OF 10 GHZ SLOTTED WAVEGUIDE ANTENNA INCORPORATED WITH MTM LENS

Here, the proposed slotted waveguide antenna incorporated with eSRR Metasurface employing MTM lens shown in Fig. 6 is analyzed, simulated and optimized using CST software. The proposed antenna operates at 10 GHz, and the metasurface structure is optimized to have a negative permeability, negative permittivity and negative refractive index in a wideband around the 10 GHz. Among high microwave frequencies X-band (8–12 GHz) makes a significant contribution to various applied and emerging wireless services [36–39]. X-band is mostly devoted to point to point wireless applications, such as on-road traffic control [36], air traffic control [37], imaging radar [36–38] and satellite communications [39], where low profile and highly directive antennas are appropriated as a reliable and economical solution for the transmission systems.

The antenna is optimized by changing the size of the metasurface and the separation between the metasurface and the slotted waveguide antenna. Figs. 7(a) and 7(b) show the return loss and radiation gain at 10 GHz of the proposed antenna at 18.5 mm separation distance h_s between the slot and the metasurface bottom side and with different slot sizes (L_s, W_s) of (14.5, 2), (14.7, 4),and (15.2, 6). The size of metasurface is $6 \times 6 \times 2$ in x, y and z directions, respectively The proposed antennas are compared with a conventional antenna of a slot size (L_s, W_s) of (15.2, 6), and all dimensions are given in mm.

It is clear from Fig. 7(a) that the radiated slot size plays an important role in widening the bandwidth of the proposed antenna. For example, the bandwidth of the proposed antenna increases from 0.854 GHz to 1.567 GHz and 2.22 GHz as the radiated slot size (L_s, W_s) is changed from (14.5, 2) to (14.7, 4), and (15.2, 6), respectively. Furthermore, as shown in Fig. 7(b), the gain of the proposed slotted waveguide antenna incorporated with NRI metasurface is increased from 6.5 dB to 10.6 dB, i.e., the E plane gain is improved by 4.1 dB, while the beamwidth decreases from 94.1 dB to about 50 dB, mostly for all the different three slots compared with their conventional slotted waveguide antenna counterparts, mostly for all slot sizes. However, the bandwidth of the proposed antenna is decreased from 2.88 GHz to 2.22 GHz compared with the conventional slotted waveguide antenna for slot dimensions (L_s, W_s) of (15.2, 6).

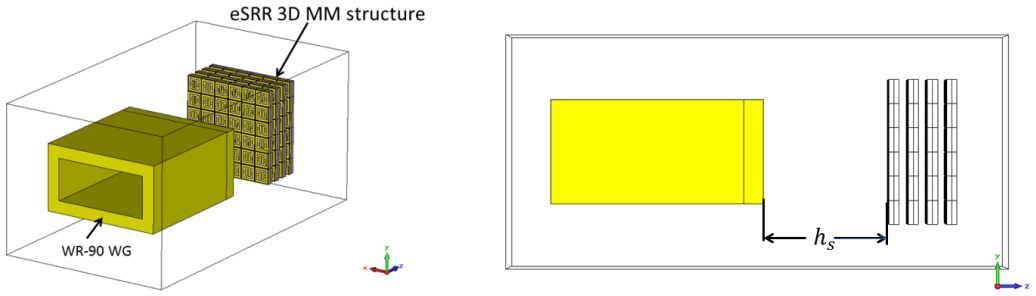

Figure 6. 10 GHz slotted waveguide antenna incorporated with eSRR NRI metasurface structure. (a) 3D view, and (b) side view.

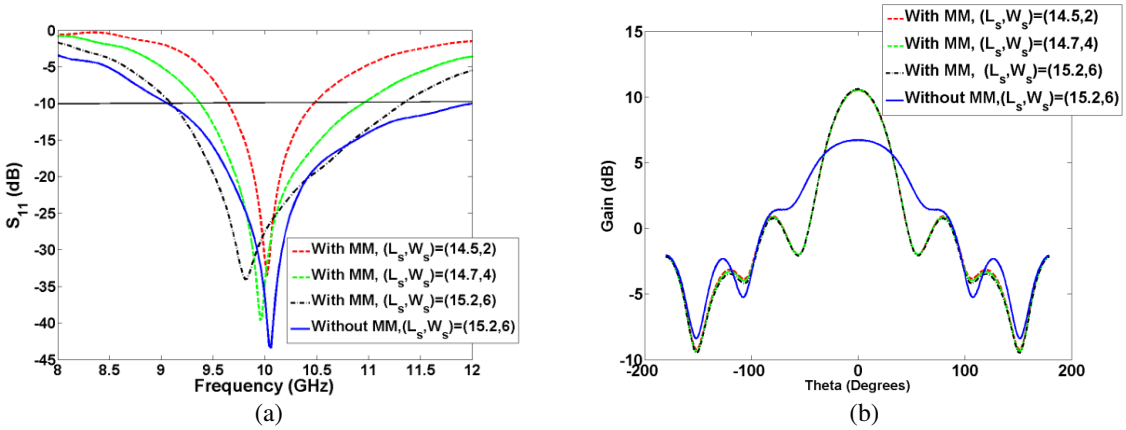

Figure 7. The simulated return loss (a) and the simulated E plane gain at 10 GHz of the proposed slotted waveguide antenna with and without eSRR metasurface with different slot sizes (L_s, W_s) of (14.5, 2), (14.7, 4),and (15.2, 6) and at 18.5 mm separation distance between the slot and the metasurface, the NRI metasurface is 3-D eSRR of $6 \times 6 \times 2$ size in x, y and z direction, respectively.

In addition, the effect of the eSRR metasurface structure size on the impedance matching, bandwidth, beamwidth and the gain of the proposed antenna is studied as shown in Fig. 8 which shows the return loss and gain of the proposed slotted waveguide antenna with and without eSRR metasurface layers. By using CST, the eSRR metasurface structure is designed with different sizes of $3\times6\times2$, $3\times6\times4$ and $6\times6\times2$ sizes in x, y and z directions, and then the separation distance h_s between the slot and the eSRR metasurface structure is changed slightly around half the free space wavelength of 15 mm at 10 GHz till the optimum impedance matching and gain are obtained. The radiated slot is of dimensions (L_s, W_s) of (14.5 mm, 2 mm) and for the size of each eSRR metasurface structure there is a corresponding separation h_s between the slot and the eSRR metasurface structure which is 21.5 mm, 22.5 mm and 18.5 mm for the eSRR metasurface structure of sizes of $3 \times 6 \times 2$, $3 \times 6 \times 4$ and $6 \times 6 \times 2$, respectively.

Figure 8(a) shows that the size of the eSRR metasurface structure and the separation distance between the slot and the eSRR metasurface structure play important roles in optimizing the impedance matching of the antenna. For example, the return loss is improved from -30 dB to about -34 dB when the size of the eSRR metasurface structure is $6\times6\times2$, and the separation distance h_s is 18.5 mm, while it becomes the worst when the size of the eSRR metasurface structure is $3 \times 6 \times 4$. However, as shown in Fig. 8(b), the E plane gain is improved from 6.5 dB to 10.5 dB when slotted waveguide antenna is incorporated with a eSRR metasurface structure of size $6 \times 6 \times 2$. It is clear that as the transverse size of the eSRR metasurface structure increases with the same number of unit cells in both x and y directions while keeping the longitudinal size, both return loss and gain are improved.

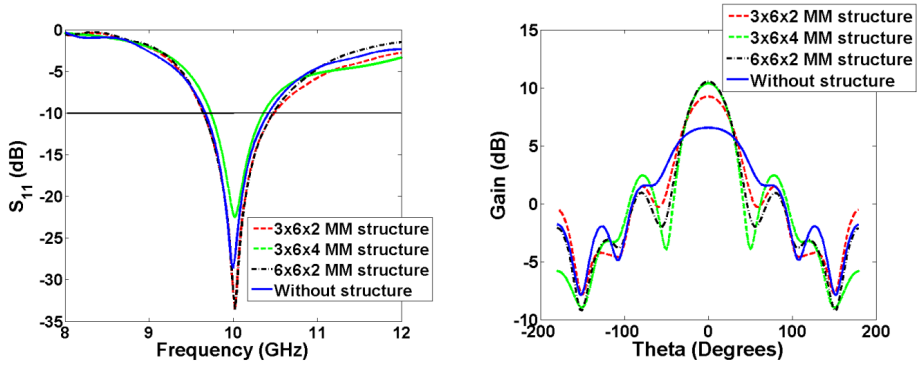

(a) (b)

Figure 8. The simulated return loss (a) and the simulated E plane gain at 10 GHz of the proposed slotted waveguide antenna with and without eSRR metasurface structure of slot sizes ($W_s L_s$) of (2 mm, 14.5 mm) and at 18.5 mm separation distance between the slot and the eSRR metasurface structure, which is 3-D eSRR metasurface of different sizes of $3 \times 6 \times 2$, $3 \times 6 \times 4$ and $6 \times 6 \times 2$ sizes in x, y and z directions.

5. FABRICATION AND MEASUREMENT

For experimental verification, the proposed antenna resonating at 10 GHz and the eSRR metasurface structure have been fabricated as shown in Fig. 9. The eSRR metasurface structure is fabricated using wet etching technique on an RT/Duroid 5880 substrate with a relative permittivity of $\varepsilon r = 2.2$ and thickness of $h = 1.57$ mm. The slotted waveguide antenna is fabricated using milling technology with the same dimensions mentioned in the previous section. Furthermore, the effect of the eSRR metasurface structure size on the antenna performance is studied using eSRR metasurface structure of sizes $6 \times 6 \times 4$ and $7 \times 7 \times 4$, placed in front of the slotted waveguide antenna at a separation distance of 18 mm. The separation distance is 5 mm from the center to the center of each two adjacent eSRR layers. The slot dimensions (W_s, L_s) are (6 mm, 15.2 mm). The return loss S_{11} for the simulated and the fabricated antenna with and without eSRR metasurface/MM is shown in Fig. 10. The measured and simulated return losses of the proposed antenna without eSRR metasurface are in agreement, and the bandwidth is about 2.88 GHz. It is important to notice that there is a shift in the center frequency, and some losses for the measured proposed antenna with mm over the simulated one due to the SMA connector, the nylon screws, and the misalignment of the eSRR stacked layers constructing the mm structure. Furthermore, the bandwidth of the proposed antenna with eSRR mm of size $7 \times 7 \times 4$ is more than that of $6 \times 6 \times 4$. This means that as the size of the eSRR metasurface structure increases, the bandwidth of the antenna increases, due to decrease of the quality factor as a result of the added conductor and dielectric losses. The bandwidth of the 10 GHz slotted waveguide antenna incorporated with MTM is increased from 22.8% to 28.8%. This increase in the bandwidth is useful for applications such as airport surveillance radar antennas which can send and receive with different frequencies in different directions [37]. It is clear from Fig. 10 that there is about 1 GHz bandwidth deviation between the simulation and measurement for the antenna incorporated with $6 \times 6 \times 4$ MTM structure due to the misalignment of the MTM layers with respect to the slotted antenna.

The simulated and measured gains versus frequency of the proposed antenna with and without mm are then plotted as shown in Fig. 11. The results show that as the size of the eSRR metasurface structure increases, the radiated wave becomes more focused due to the NRI property, and hence the antenna directivity increases. Although the eSRR metasurface structure adds more loss to the antenna which degrades the radiation efficiency, the overall gain of the antenna increases due to the significant increase in the antenna directivity over its efficiency. The antenna gain increases from about 6 dB to 11 dB at 10 GHz. There is a deviation between the measured and simulated results due to the losses presented by the connectors, nylon spacers, metal nuts and misalignment of the eSRR layers.

It is clear that although the MTM has a good transmission around 10 GHz, and the allotted

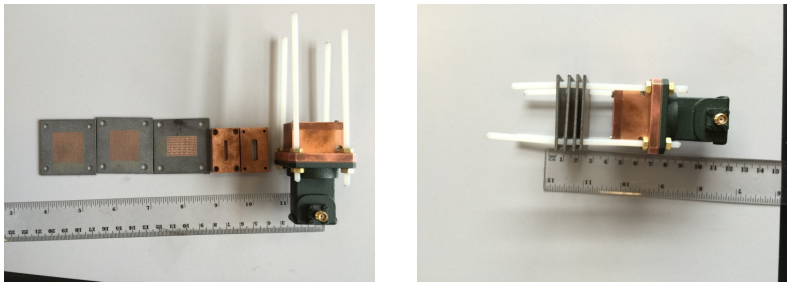

(a) (b)

Figure 9. The fabricated antenna, (a) conventional slotted waveguide antenna on the right, other two slots in the centre and eSRR metasurfaces of sizes $6 \times 4 \times 1$, $6 \times 6 \times 1$ and $7 \times 7 \times 1$ from right to left, and (b) slotted waveguide antenna incorporated with eSRR 3D structure of size $6 \times 6 \times 4$ located at a distance h_s of 18 mm from the slot and the separation distance is 5 mm from the centre to the centre of each two adjacent eSRR layers.

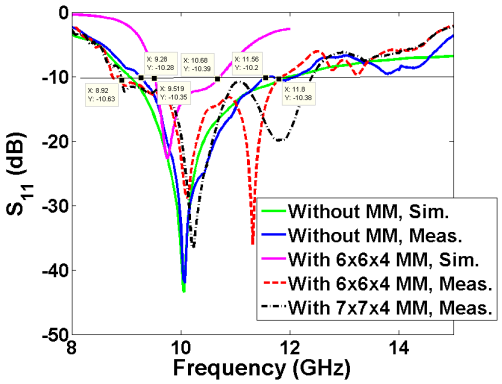

Figure 10. Simulated and measured s-parameter magnitudes of the slotted waveguide antenna with and without eSRR metasurface structure of sizes $6 \times 6 \times 4$ and $7 \times 7 \times 4$, located at a distance h_s of 18 mm from the slot and the separation distance is 5 mm from the centre to the centre of each two adjacent eSRR layers.

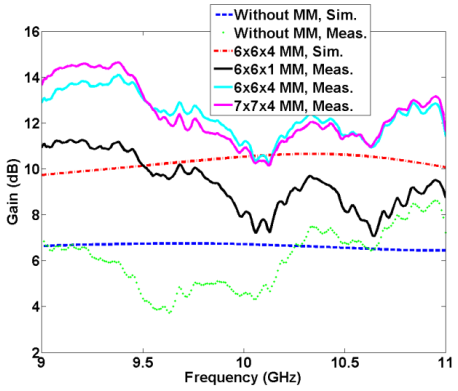

Figure 11. Comparison between the measured and the simulated gains of the proposed antenna with and without eSRR metasurface structure of sizes $6 \times 6 \times 4$ and $7 \times 7 \times 4$, located at a distance h_s of 18 mm from the slot and the separation distance is 5 mm from the centre to the centre of each two adjacent eSRR layers.

waveguide antenna has a good impedance matching at 10 GHz, the slotted waveguide antenna peak gain does not occur at 10 GHz as shown in Fig. 11. The main reason behind shifting the peak gain of the designed antenna away from 10 GHz for the measured proposed antenna is that the reference antenna used to measure the designed antenna S_{21} parameter is linearly polarized, and at the same time the MTM layers placed in front of the slotted antenna can slightly change the polarization of the antenna due to the misalignments between the different layers of MTM and/or between the MTM layers and the slotted antenna. The mismatching between the polarizations of the measured antenna and the reference antenna may cause shift in the transmission peak between the two antennas as shown in Fig. 11. As a future work, this problem can be solved by using a more precise alignment tools in the construction of the prototyped antenna.

Furthermore, E and H plane radiation patterns at 10 GHz of the simulated and measured proposed antennas with and without eSRR metasurface structure are plotted as shown in Fig. 12 for different eSRR metasurface structure sizes and at a separation distance of 18 mm between the MM structure and the slot edge. It is clear that as the eSRR metasurface structure size is increased from $6 \times 6 \times 1$ to $7 \times 7 \times 4$, the radiation pattern becomes more focused, and the beamwidth decreases in both E and H planes. However, there is a nice agreement between the measured and simulated results.

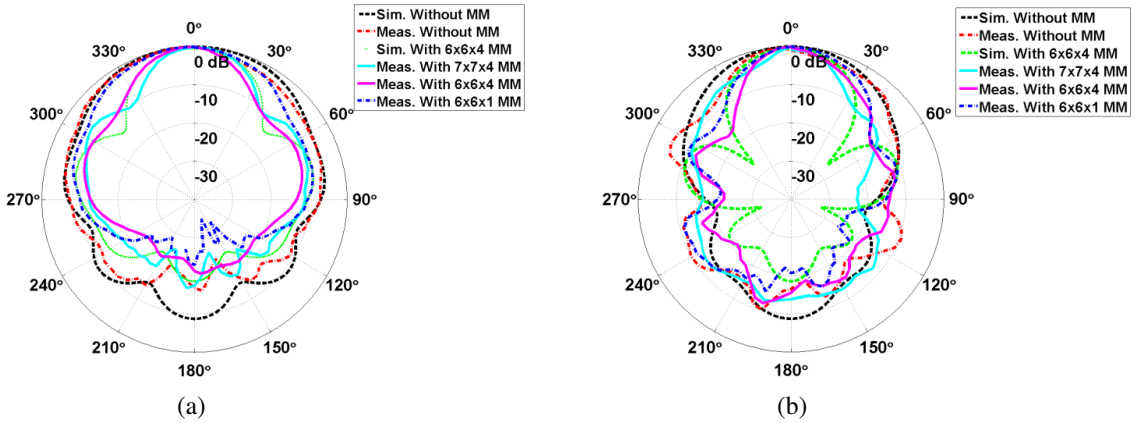

Figure 12. Measured and simulated radiation pattern at 10 GHz of the proposed with and without eSRR metasurface structure of sizes $6 \times 6 \times 1$, $6 \times 6 \times 4$ and $7 \times 7 \times 4$, located at a distance h_s of 18 mm from the slot and the separation distance is 5 mm from the centre to the centre of each two adjacent eSRR layers, (a) E-plane and (b) H-plane.

6. CONCLUSION

In this paper, a new slotted waveguide antenna incorporated with eSRR metasurface structure employing a NRI medium is proposed, designed, simulated in CST, fabricated and measured. The major advantage of the proposed slotted waveguide antenna over the high gain conventional horn antennas is that it is uses planner metasurface structure with NRI property for beam focusing purposes of the radiated EM waves and hence antenna gain can be improved. The proposed MTM structure in this paper can be designed at THz frequencies by using different materials.

The proposed antenna is constructed from a back side slotted waveguide antenna incorporated with 2-D eSRR metasurface structure arranged as sacked layers with 5 mm separation distance between each two layers, then the 3D eSRR metasurface structure is placed in front of the slotted antenna with a separation distance about half the free space wavelength. The proposed antenna is designed and optimized in CST, and the impact of the eSRR metasurface structure size and the separation distance between the eSRR metasurface structure and the slotted antenna on the antenna performance are studied. The slotted waveguide antenna is fabricated using the milling technology, and the eSRR metasurface structure is fabricated using the wet etching technology. The return loss, gain and radiation pattern in both E and H planes are measured. The simulated and measured results are compared. The results show a good agreement between the simulation and measurement. The antenna gain is improved from 6.5 dB to 11 dB; the beam is reduced from 94.1 degrees to about 50 degrees in E plane, while the bandwidth and return loss are slightly changed.

As a future work, the idea of gain improvement of the slotted waveguide incorporated with the eSRR metasurface structure can be extended to THz frequency range to be used for short distance wireless communication links, particularly in the biomedical application and inside the satellite to reduce the wiring complexity of the satellite system. Also, eSRR metasurface structure can replace the bulky silicon lens used in THz photoconductive and photo mixer optical antennas to focus the radiated beam and improve the antenna gain for medical applications [40, 41].

REFERENCES

1. Kang, M., N. H. Shen, J. Chen, J. Chen, Y. X. Fan, J. Ding, and P. Wu, "A new planar left-handed metamaterial composed of metal-dielectric-metal structure," *Optics Express*, Vol. 16, No. 12, 8617–8622, 2008.
2. Luk'yanchuk, B., N. I. Zheludev, S. A. Maier, N. J. Halas, P. Nordlander, H. Giessen, and C. T. Chong, "The Fano resonance in plasmonic nanostructures and metamaterials," *Nature materials*, Vol. 9, No. 9, 707–715, 2010.

3. Omelyanovich, M., V. Ovchinnikov, and C. Simovski, "A non-resonant dielectric metamaterial for the enhancement of thin-film solar cells," *Journal of Optics*, Vol. 17, No. 2, 025102, 2015.
4. Pendry, J. B., "Negative refraction makes a perfect lens," *Physical Review Letters*, Vol. 85, No. 18, 3966, 2000.
5. Zharov, A. A., N. A. Zharova, R. E. Noskov, I. V. Shadrivov, and Y. S. Kivshar, "Birefringent left-handed metamaterials and perfect lenses for vectorial fields," *New Journal of Physics*, Vol. 7, No. 1, 220, 2005.
6. Grbic, A. and G. V. Eleftheriades, "A backward-wave antenna based on negative refractive index LC networks," *IEEE Antennas and Propagation Society International Symposium*, Vol. 4, 340–343, 2002.
7. Grbic, A. and G. V. Eleftheriades, "Experimental verification of backward-wave radiation from a negative refractive index metamaterial," *Journal of Applied Physics*, Vol. 92, No. 10, 5930–5935, 2002.
8. Chen, X., H. F. Ma, X. M. Yang, Q. Cheng, W. X. Jiang, and T. J. Cui, "X-band high directivity lens antenna realized by gradient index metamaterials," *Proc. Asia Pac. Microw. Conf. (APMC)*, Vols. 1–5, 793–797, 2009.
9. Yuan, Y., C. Bingham, T. Tyler, S. Palit, T. H. Hand, W. J. Padilla, N. M. Jokerst, and S. A. Cummer, "A dual-resonant terahertz metamaterial based on single-particle electric-field-coupled resonators," *Appl. Phys. Lett.*, Vol. 93, No. 19, 191110, 2008.
10. Landy, N. I., S. Sajuyigbe, J. J. Mock, D. R. Smith, and W. J. Padilla, "Perfect metamaterial absorber," *Phys. Rev. Lett.*, Vol. 100, No. 20, 207402, 2008.
11. Chin, J. Y., J. N. Gollub, J. J. Mock, R. P. Liu, C. Harrison, D. R. Smith, and T. J. Cui, "An efficient broadband metamaterial wave retarder," *Opt. Express*, Vol. 17, No. 9, 7640–7647, 2009.
12. Chen, X., H. F. Ma, X. M. Yang, Q. Cheng, W. X. Jiang, and T. J. Cui, "X-band high directivity lens antenna realized by gradient index metamaterials," *Proc. Asia Pac. Microw. Conf. (APMC)*, Vol. 1–5, 793–797, 2009.
13. Xiao, Z. G. and H. L. Xu, "Low refractiveMTMs for gain enhancement of horn antenna," *J. Infrared Millimeter Terahertz Waves*, Vol. 30, No. 3, 225–232, 2009.
14. Vaidya, A. R., R. K. Gupta, S. K. Mishra, and J. Mukherjee, "Efficient, high gain with low side lobe level antenna structures using parasitic patches on multilayer superstrate," *Microwave and Optical Technology Letters*, Vol. 54, No. 6, 1488–1493, 2012.
15. Choi, W., Y. H. Cho, C. S. Pyo, and J. I. Choi, "A high-gain microstrip patch array antenna using a superstrate layer," *ETRI Journal*, Vol. 25, No. 5, 407–411, 2003.
16. *Parabolic Reflector Antennas*, U.S. Patent 3,572,071, issued March 23, 1971.
17. Pendry, J., "Negative refraction makes a perfect lens," *Phys. Rev. Lett.*, Vol. 85, No. 18, 4166–4169, 2000.
18. Islam, M. M., M. T. Islam, M. Samsuzzaman, M. R. I. Faruque, N. Misran, and M. F. Mansor, "A miniaturized antenna with negative index metamaterial based on modified SRR and CLS unit cell for UWB microwave imaging applications," *Materials*, Vol. 8, No. 2, 392–407, 2015.
19. Alibakhshi-Kenari, M. and M. Naser-Moghadasi, "Novel UWB miniaturized integrated antenna based on CRLH metamaterial transmission lines," *AEU-International Journal of Electronics and Communications*, Vol. 69, No. 8, 1143–1149, 2015.
20. Enoch, S., G. Tayeb, P. Sabouroux, N. Guérin, and P. Vincent, "A metamaterial for directive emission," *Physical Review Letters*, Vol. 89, 213902, 2002.
21. Xu, H., Z. Zhao, Y. Lv, C. Du, and X. Luo, "Metamaterial superstrate and electromagnetic band-gap substrate for high directive antenna," *Int. J. Infrared Milli Waves*, Vol. 29, 493–498, 2008.
22. Ju, J., D. kim, W. J. Lee, and J. I. Choi "Wideband high-gain antenna using metamaterial superstrate with the zero refractive index," *Microwave and Optical Tech. Lett.*, Vol. 51, No. 8, 1973–1976, 2009.
23. Temelkuaran, B., M. Bayindir, E. Ozbay, R. Biswas, M. Sigalas, G. Tuttle, and K. M. Ho, "Photonic crystal-based resonant antenna with a very high directivity," *Journal of Applied Physics*, Vol. 87,

603–605, 2000.

24. Alù, A., F. Bilotti, N. Engheta, and L. Vegni "Metamaterial covers over a small aperture," *IEEE Trans. Antennas Propag.*, Vol. 54, No. 6, 1632–1643, June 2006.
25. Tang, M., S. Xiao, D. Wang, J. Xiong, K. Chen, and B. Wang, "Negative index of reflection in planar metamaterial composed of single split-ring resonators," *Applied Computational Electromagnetics Society (ACES) Journal*, Vol. 26, No. 3, 250–258, March 2011.
26. Averitt, R. D., W. J. Padilla, H. T. Chen, J. F. O'Hara, A. J. Taylor, C. Highstrete, and A. C. Gossard, "Terahertz metamaterial devices," *Optics East 2007 (677209-677209), International Society for Optics and Photonics*, September 2007.
27. Maritz, A. J. N., "Investigation and design of a slotted waveguide antenna with low 3D sidelobes," Doctoral dissertation, Stellenbosch University, 2010.
28. Mahmud, R., T. He, M. Lancaster, Y. Wang, and X. Shang, "Micromachined travelling wave slotted waveguide antenna array for beam-scanning applications," 2014.
29. Li, Y., I. Mehdi, A. Maestrini, R. H. Lin, and J. Papapolymerou, "A broadband 900-GHz silicon micromachined two-anode frequency tripler," *IEEE Transactions on Microwave Theory and Techniques*, Vol. 59, No. 6, 1673–1681, 2011.
30. Grabowski, M., "Non-Resonant Slotted Waveguide Antenna Design Method," *High Frequency Electronics*, 2012.
31. Chen, X., T. Grzegorczyk, B. Wu, J. Pacheco, and J. Kong, "Robust method to retrieve the constitutive effective parameters of metamaterials," *Physical Review E*, Vol. 70, No. 1, 2004.
32. Arslanagic, S., T. V. Hansen, N. A. Mortensen, A. H. Gregersen, O. Sigmund, R. W. Ziolkowski, and O. Breinbjerg, "A review of the scattering-parameter extraction method with clarification of ambiguity issues in relation to metamaterial homogenization," *IEEE Antennas and Propagation Magazine*, Vol. 55, No. 2, 91–106, 2013.
33. Nicolson, A. M. and G. F. Ross, "Measurement of the intrinsic properties of materials by time-domain techniques," *IEEE Transactions on Instrumentation and Measurement*, Vol. 19, No. 4, 377–382, 1970.
34. Boughriet, A. H., C. Legrand, and A. Chapoton, "Noniterative stable transmission/reflection method for low-loss material complex permittivity determination," *IEEE Transactions on Microwave Theory and Techniques*, Vol. 45, No. 1, 52–57, 1997.
35. Campione, S., S. Steshenko, M. Albani, and F. Capolino, "Complex modes and effective refractive index in 3D periodic arrays of plasmonic nanospheres," *Optics Express*, Vol. 19, No. 27, 26027-26043, 2011.
36. Carrasco, E., M. Barba, and J. Encinar, "X-band reflectarray antenna with switching-beam using pin diodes and gathered elements," *IEEE Trans. Antennas Propag.*, Vol. 60, No. 12, 5700–5708, 2012.
37. Vallecchi, A. and G. B. Gentili, "A shaped-beam hybrid coupling microstrip planar array antenna for X-band dual polarization airport surveillance radars," *The Second European Conf. on Antennas and Propagation, 2007, EuCAP 2007*, 1–7, November 2007.
38. Kuo, F. Y. and R. B. Hwang, "High-isolation X-band marine radar antenna design," *IEEE Trans. Antennas Propag.*, Vol. 62, No. 5, 2331–2337, 2014.
39. Jung, E. Y., J. W. Lee, T. K. Lee, et al., "SIW-based array antennas with sequential feeding for X-band satellite communication," *IEEE Trans. Antennas Propag.*, Vol. 60, No. 8, 3632–3639, 2012.
40. Kurzweil-Segev, Y., M. Brodsky, A. Polsman, E. Safrai, Y. Feldman, S. Einav, and P. Ben Ishai, "Remote monitoring of phasic heart rate changes from the palm," *IEEE Transactions on Terahertz Science and Technology*, Vol. 4, No. 5, 618–623, 2014.
41. Sun, M., Z. N. Chen, H. Tanoto, Q. Y. Wu, J. H. Teng, and S. B. Yeap, "Design of continuous-wave photomixer driven terahertz dipole lens antennas," *APSIPA Annual Summit and Conference*, 14–17, December 2010.